International Journal of Current Advanced Research
ISSN: O: 2319-6475, ISSN: P: 2319-6505, Impact Factor: SJIF: 5.995
Available Online at www.journalijcar.org
Volume 6; Issue 12; December 2017; Page No. 8249-8256
DOI: http://dx.doi.org/10.24327/ijcar.2017.8256.1320

Research Article

MORPHOLOGY AND SENSOR PROPERTY OF POLYANILINE/$CuCeO_2$ NANOCOMPOSITES

Rajashekhar Badiger[1]., Vishnuvardhan T K*[2]., Satishkumar K B[3]., Shashidhar*[1]., Basavaraja C[4] and Vijaykumar RK[5]

[1]Department of Chemistry, SDM College of Engineering & Technology, Dharwad-580002, Karnataka, India
[2]Department of Chemistry, 470, IV Phase, Peenya, Ramaiah University of Applied Sciences Bangalore-58, Karnataka, India
[3]Department of Chemistry, Acharya Institute of Technology, Soladevana Halli, Bangaluru- 585 106 Karnataka, India
[4]Department of Chemistry, Inje University, Kyungnam-621-749, South Korea
[5]Department of Chemistry, Gulbarga University, Gulbarga-592-585, Karnataka, India

A R T I C L E I N F O

Article History:
Received 16th September, 2017
Received in revised form 25th October, 2017
Accepted 19th November, 2017
Published online 28th December, 2017

Key words:
Nanoparticles, nanocomposites, AC conductivity, dielectric properties, sensor activity.

A B S T R A C T

Polyaniline and PANI/$CuCeO_2$ nanocomposites are synthesized by in situ chemical oxidative polymerization of aniline monomer by incorporating $CuCeO_2$ nanoparticles using Ammonium persulphate as oxidant and Dodecyl Benzene Sulphonic Acid as surfactant at 0-5 ^{0}C. Different weight percentages of $CuCeO_2$ (5%, 10%, 15%, 20%) are used during in situ polymerization. The nanocomposites are characterized by Fourier Transform Infrared and X-Ray DiffractionTechniques. Surface morphology is studied using Scanning Electron Microscopy. Frequency dependent AC conductivity and dielectric properties of PANI/$CuCeO_2$ nano-composites are analyzed in the frequency range from 50 Hz to 5 MHz at room temperature. The study of AC conductivity reveals that the presence of $CuCeO_2$ enhances the conductivity and dielectric properties of the nanocomposites. The gas sensing properties were studied towards gases like ammonia, carbon dioxide, methanol and it is observed that the nanocomposite PDC-15 show maximum sensitivity at 130 ^{0}C temperatures.

INTRODUCTION

Electrically conducting polymers deserve significance in present technology since they have potential applications in optical and micro-electronic devices, chemical sensors, catalysis, and energy storage systems[1]. Polyaniline(PANI), the most extensively studied electrically conducting polymer, has been widely investigated for electronic/electrical applications due to its good environmental stability,ease of synthesis, excellent electrical, optoelectrical,photovoltaic and dielectric properties[2-7]. But it suffers from poor mechanical properties and low processibility. To overcome these problems, the polymer is incorporated with metal or metal oxide or metal sulphide to form Polymer/metal or Polymer/metal oxide or Polymer/metal sulphide composites. Polymer metal oxide composites possess unique electrical properties [8]. Polymer/metal oxide composites which are organic/inorganic hybrids[9] have attracted much attention due to their potential applications in many areas, such as thin-film field-effect transistors, batteries and solar cells. They provide better electrical properties due to the direct interfacial interaction of polymers within organic materials like metal oxide nanoparticles (NP) where the polymers act as donors and inorganicparts as acceptors[10]. One such metal oxide which can give desired properties to Polyaniline is Ceria(CeO_2). CeO_2 nanoparticles[11] are presumed to be excellent photocatalysts[12] because of their strong redox ability and they are preferred for their low cost[13]. To prepare ceria nanoparticles various solution based methods are employed such as coprecipitation, hydrothermal, sol-gel and solution combustion [14] methods. Ceria nanoparticles obtained from most of these methods have reduced surface area[about 100 m^2/g]. The minimum temperature of 973 K which is used in these above methods to reduce the loss of surface area[15]. To minimize this reduction of surface area, ceria is doped with rare earth or transition metal[16] such as Cu, Ni, Fe etc which also enhances the redox ability of ceria[17]. Ceria based composites such as $CuCeO_2$ nanocomposites (CCN) find wide applications as solid electrolytes, solar cells, fuel cells, sensors[18-20]etc.

The interest in Cu-NPs is increasing now-a-days due to its useful properties (thermal and electrical conductivity), which is achieved at much lower cost compared to other noble metals

Corresponding author:* **Shashidhar
Department of Chemistry, SDM College of Engineering & Technology, Dharwad-580002, Karnataka, India

like silver and gold [21]. However, the major limitations in the synthesis of Cu-NPs are their ease of oxidation to CuO or Cu_2O during preparation and storage [22]. This limitation is overcome by applying urea gelation co-precipitation(UGC) method to prepare metal oxides [23]. One more problem with the stability of polyaniline/$CuCeO_2$ composites is the weak linkage between PANI and CCN which hinders the aim of getting good processable polymer composite with better properties. To ensure a strong linkage between PANI and CCN, use of surfactants is made. Surfactants such as Dodecyl Benzene Sulphonic Acid (DBSA), Sodium Dodecyl Benzene Sulphonic Acid (SDS), Camphor Sulphonic Acid(CSA) etc., play an important role in the synthesis of conducting polymers. They help binding the CCN with PANI molecules apart from increasing the processability [24] and to some extent even the conducting properties of PANI, accompanied by structural and morphological changes [25]. The recent work by Parveen and Veena shows that the doping level is highest when the surfactant used is DBSA in the synthesis of PANI as compared with other surfactants like CSA, Lignin-Sulphonic-Acid (LSA), and Cardanolazo-Phenyl- Sulphonic-Acid (CDSA) [26]. Most of the sensor property is studied with respect to metal oxides[27]. Though inorganic semiconducting metal oxides (SMO) such as TiO_2,SnO_2,WO_3 etc are used as good sensors due to low cost, better sensitivity, simple sensitivity methods[30], they consume more power because of high working temperatures[28]. To overcome this problem, Conducting polymers (CP) such as polythiophene(PT), polypyrrole (PPy), polyaniline (PANI) [29] etc which operate at room temperature are preferred[30,31]. They are also considered due to ease of deposition onto a wide variety of substrates and their rich structural modification chemistry[32]. But still the CPs suffer from drawbacks such as low thermal stability, low response, long response time to gas sensors[33]. Hence CPs blended with nano-metal oxides are considered to be the best candidates suited for sensor applications which overcome these problems[34-36].

In this work, report the synthesis of polyaniline/$CuCeO_2$(PDC) nanocomposites by the method of inorganic/organic interfacial synthesis technique using a surfactant DBSA and study of their electrical and sensor properties. The physical characteristicsof the resulting products are investigated thoroughly via UV-visible absorption studies, X-ray diffraction(XRD), Fourier transform infrared spectroscopy(FTIR). Williamson-Hall (WH) method is used for justifying crystallite size determined by using Scherrer Equation and crystallite strain which is obtained from the peak width analysis. Scanning electron microscopy (SEM) studies and Frequency dependent AC conductivity studies of prepared nanocomposites are made. Sensor activity of PDC nanocomposites is studied by taking NH_3, $CO_2$and CH_3OH as the test gases.

Experimental

MATERIALS AND METHOD

Copper Nitrate and Ceric Ammonium Nitrate(both Hi-media), Monomer Aniline (used after distillation) and HCl both purchased from Merck, Ammonium persulphate(APS) and Urea both purchased from sd-fine, ethanol(anhydrous)(Nice chemicals) and DBSA(Hi-media). All chemicals used are of AR grade.

$CuCeO_2$ nanoparticles synthesis

(i) formation of a slurry by combining ceria nano particles with copper 2,4-pentanedionate in an aqueous suspension; (ii) above formed slurry is heated to a suitable temperature for sufficient time to decompose the slurry composite in presence of oxygen-argon atmosphere to form nanoparticles of copper ceria.(iii) copper ceria nano particles are heat treated to oxidize some of the copper nanoparticles to copper oxide nanoparticles optionally. Precursors used in urea gelation co-precipitation (UGC) method are copper nitrates and ceric ammonium nitrates$(NH_4)_2Ce(NO_3)_6$. Urea as a fuel mixed with precursor salts are stirred vigorously and heated at 100 ^{0}C for 8 hours with the addition of de-ionized water to get co-precipitate of Cu-CeO_2 nanoparticles.The precipitate is filtered, washed and dried in oven for 10-12 hours. The product is calcined for 4-6 hours slowly[23].

Synthesis of PANI/$CuCeO_2$ nano composites

A known amount of concentration of $CuCeO_2$(weight%) is dispersed in de-ionised water and the mixture is stirred for about 30 minutes to achieve uniform dispersion. With continued stirring a 50ml of 0.05 mole DBSA is added as surfactant so that the surfactant molecules attached to the surface of $CuCeO_2$ nanoparticles to form some kind of $CuCeO_2$-DBSA complex. Then 0.06M of monomer is added slowly with continued stirring. The suspension is then stirred magnetically for 3 hours. Later 0.1 M Ammonium persulfate is added drop wise with stirring and the reaction mixture is allowed for about 4-5 hours so that the aniline monomer polymerize on the surface of $CuCeO_2$-DBSA complex at the temperature 0-5^{0}C to form PANI/$CuCeO_2$ nanocomposite. The above composite is filtered, washed with de-ionised water repeatedly and then with 5% ethanol to remove excess of APS and unreacted DBSA and aniline monomer. The pure polymer PANI is prepared using the same procedure without the addition of NPs.

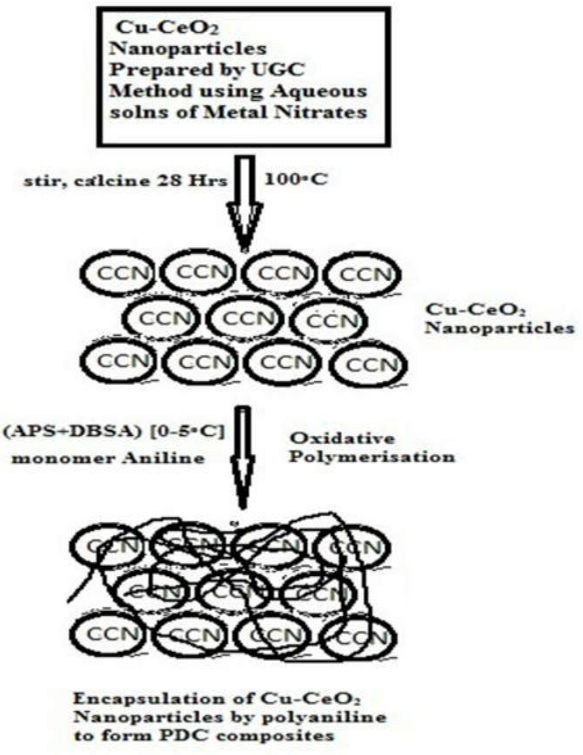

Figure 1 Schematic Diagram showing the synthesis of PDC nanocomposites.

The concentration of CuCeO2 NP is varied as weight percentages of 5%, 10%, 15% and 20% in the preparation of PANI/$CuCeO_2$ nanocomposite and the composites are labeled as PDC-5, PDC-10, PDC-15 and PDC-20 respectively. Scheme for the synthesis of PANI/$CuCeO_2$ are depicted in Fig. *1*.

Instrumentation and Characterization

The optical absorption spectra are carried out using Shimadzu UV-1700E double beam UV-VIS spectrophotometer in the range of 200 nm to 800 nm. For the analysis of functional groups in the synthesized polymer composites, FTIR spectra are performed on Bruker Optic GMBH Tensor27 Spectrophotometer using KBr pellet technique in the wavelength range of 4000-400 cm^{-1}. XRD analysis is carried on Bruker D2 Phraser automatic X-ray diffractometer with Cu-Kα radiation (λ=1.54Å), from $2\theta=10^0$-80^0 with a scanning speed of 10° min^{-1}. SEM images are obtained using GEMINI ULTRA 55with Resolution 2.4Å**.**

RESULTS AND DISCUSSIONS

UV-visible absorption studies

UV-vis spectra provide the information for understanding the electronic structure of the composites. Fig.2 depicts the UV-vis spectra of PANI-10% $CuCeO_2$, PANI-15% $CuCeO_2$ dispersed in ethanol. All the absorbance peaks observed at approximately 204, 220, 221, 247 and 372 nm are similar to the PANI peaks reported [37]. The UV-vis spectra of the PDC-10, PDC-15 polymer composites show the absorbance bands pertaining to PANI and $CuCeO_2$**.** The characteristic absorption band observed in the spectrum of PANI at 372 nm wavelength is attributed to benzenoid to quinoid excitonic transitioni.e.,(π-π^*) transition. This show complete transformation of emeraldine salt to the emeraldine base form.

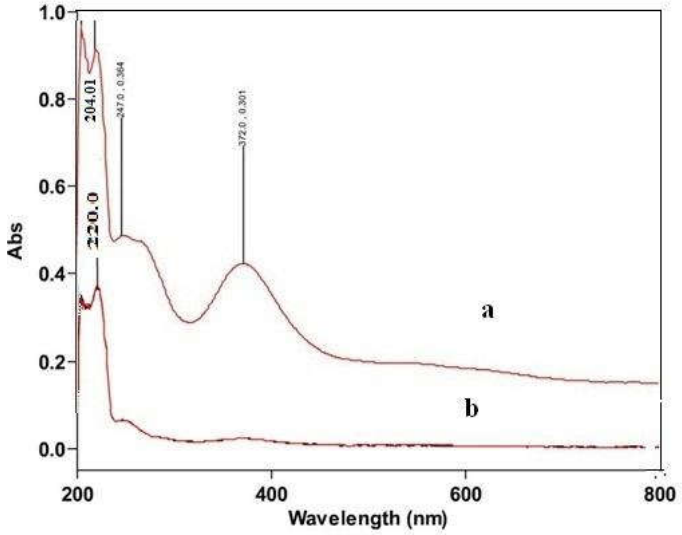

Figure 2 UV-visible spectra of a) PDC-10b) PDC-15.

Fourier Transform Infrared Spectral Studies

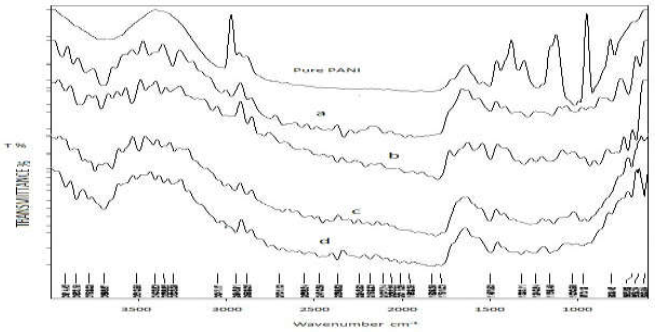

Figure 3 FTIR spectra of Pure PANI and a)PDC-5 b) PDC-10c) PDC-15 and d) PDC-20.

Fig.3 shows the FTIR spectra of PANI and PANI-$CuCeO_2$ nanocomposites. FTIR spectra of PANI show characteristic transmission peaks at 3458, 1591, 1497, 1309, 1240, 1148 and 810 cm^{-1}. The peak at 3458 cm^{-1}can be attributed to N-H stretching mode. The bands at 1591 and 1497 cm^{-1}can be attributed to stretching vibrations of quinoid-type rings and benzenoid-type rings. The bands at 1591 and 1497 cm^{-1} can be attributed to nonsymmetrical C=C stretching vibrations in the quinoid-type and benzenoid-type rings. The band at 1309 cm^{-1}corresponds to C-N stretching in quinoid form of oxidized PANI. Peak at 1240 cm^{-1}may be assigned to C-N stretching in benzenoid ring of conducting protonated form of PANI. Presence of secondary aromatic amine and its C-N stretching reveals small absorption peak at 1148 cm^{-1}. The out-of-plane bending vibration of C-H on the para-disubstituted aromatic rings may be assigned at peak at 810 cm^{-1}[37].

X-Ray Diffraction Studies

X-ray diffraction patterns of $CuCeO_2$ and its PANI composites are shown in Fig.4 The fluorite-type structure for $CuCeO_2$ are confirmed by diffraction lines are in congruent with the reported work by R.K. Pati *et.al*.,[15]**.** The characteristic peaks are observed at 2θ=28.75, 33.27, 47.68, 56.54, 59.3. The crystallite structures show the presence of peaks corresponding to the planes (111), (200), (220), (311) and (222) out of which first three planes match with Ceria NP and the remaining with CuNPs. It is noted that XRD values are in good agreement with the literature (JCPDS file for ceria: 34-0394, and for Cu : 05-661). Along with these peaks there are some broad peaks which represent the presence of PANI.

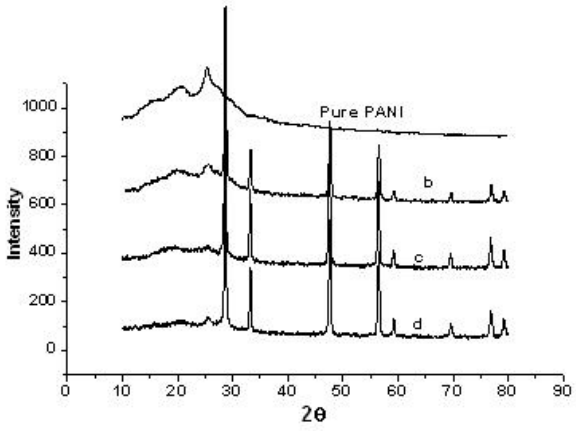

Figure 4 XRD pattern of Pure PANI andb) PDC-10c) PDC-15 d) PDC-20.

The size CNp and its composites are calculated and tabulated in Table 1 from Scherrer Equation

$$D = \frac{k\lambda}{\beta\cos\theta} \qquad ----------1.$$

Where, λ,θ,D, β and k is the wavelength of the radiation(=1.54 Å), peak position, the particle size in nm,the Full Width at Half Maximum intensity and constant equal to 0.9 respectively. Particle size and strain induced broadening are calculated by Williamson-Hall method (WH method) [38]. Graph is plotted with βcosθ Vs 4sinθ and slope is determined and the particle size calculated which is in good agreement with Scherrer Equation values are given in Table 1. The particle size calculation is done for planes (111), (200), (220). Further, size-strain plot model for each of the synthesized PDC composites, the strain induced broadening value in the order of 0.326 to 0.651 is calculated from WH plot. It is found that the strain induced in composites depending on their size during polymerization varies from one composite to another. In this study it is observed that as the crystallite size of particle depends on strain induced in the composites.

Table 1 Comparison of particle size as calculated from Scherrer Equation and WH plots and strain induced broadening using XRD pattern for PDC-composites

Sl.No.	Composite	Average Particle size from Scherrer Equation	Particle size from Williamson-Hall method	Strain induced broadening
1	PDC-10	55.63 nm	47.80 nm	0.651
2	PDC-15	64.94 nm	59.74 nm	0.326
3	PDC-20	63.43 nm	56.80 nm	0.435

SEM

Fig. 5 depicts SEM images of 15K Magnification for PDC-5, PDC-10, PDC-15 and PDC-20 nanocomposites. Fig. 5a shows needle shaped and granules like structures of the composites. Fig. 5b shows the encapsulation of nanoparticles by polyaniline. Fig.5c for PDC-15 shows agglomeration of composites with structures resembling flower like formation. Fig.5d for PDC-20 shows spherical shaped structures with cluster formation.

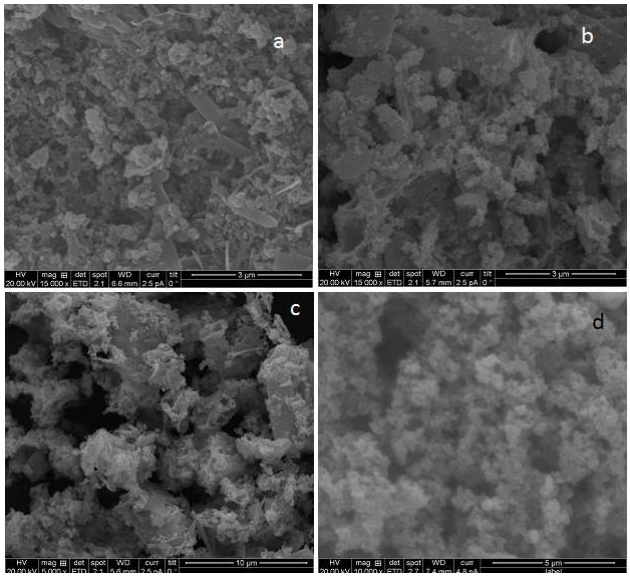

Figure 5 SEM images for a) PDC-5 b) PDC-10c) PDC-15 d) PDC-20.

Study of Electrical Properties

Conductivity Studies

Conductivity of polymer composites is dependent on the structural disorder of samples and doping procedure [39]. The frequency dependent AC conductivity at room temperature for PANI (inset) and PDC composites is shown in Fig.6 The conductivity of PANI which resumes at 4.490×10^{-5} S/cm at room temperature at 50 Hz goes upto 1.9058 S/cm at same temperature at 5 MHz changes from 5.6272×10^{-4} S/cm at room temperature at 50 Hz to 8.87 S/cm at same temperature at 5 MHz after incorporation of $CuCeO_2$. Conductivity of PANI and PANI composites remains same upto the frequency of 10^5 Hz after which there is sharp rise in the conductivity at higher frequency. As shown in the spectral and morphological studies, a strong interaction exists between the quinoid ring structures of PANI and $CuCeO_2$ in PANI/$CuCeO_2$ nanocomposites. Therefore, $CuCeO_2$ can act as a charge transport system between PANI domains within the PANI composite matrix, which leads to the increased electrical conductivities of the PANI/$CuCeO_2$ nanocomposites. Maximum conductivity is shown by PDC-15 composite. The total conductivity usually depends upon two important factors viz., Microscopic conductivity and Macroscopic conductivity [40]. The microscopic conductivity depends upon the doping level, conjugation length or chain length etc, inhomogeneities in the

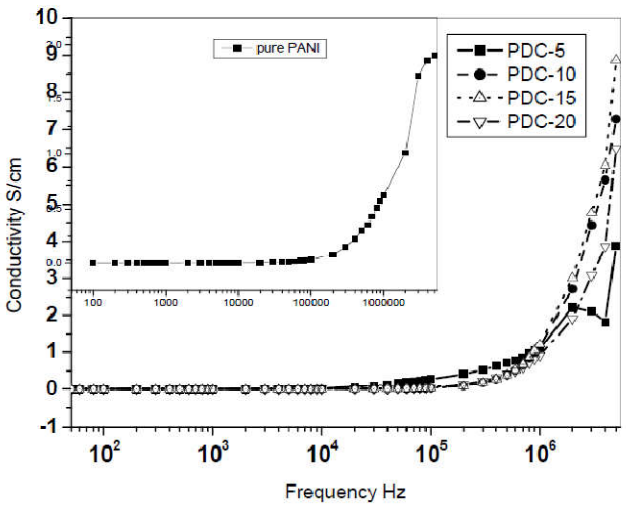

Figure 6 Frequency dependent AC conductivity of PANI (inset figure) and PANI composites a)PDC-5 b) PDC-10 c) PDC-15 d)PDC-20.

composites explains the macroscopic conductivity, compactness of pellets, orientation of particles etc. The PANI/$CuCeO_2$nanocomposites are in homogeneous because of dispersion of $CuCeO_2$ particles in the polymer composites. In the present study, the nanocomposites are synthesized in identical conditions by *in situ* polymerization of aniline in the presence of $CuCeO_2$. Hence the similar microscopic conductivities are retained. However, there is a possibility of variation in the physical (macroscopic) properties viz. compactness and molecular orientations, owing to the variation in the weight percentage of $CuCeO_2$in the composites. Microcrystalline nature of oxide particles can enhance the orderness in the composites, which is confirmed from XRD. The conductivity of the composites also increases with reduction in the strain induced broadening which is evident from the WH plots.

Dielectric Properties: Dielectric Constant

The variation of Dielectric Constant of the PDC composites as a function of frequency from 50 Hz to 5 MHz at room temperatureis shown in the Fig.7. At lower frequency PDC-15 sample shows higher dielectric constant. All the composites show saturated dielectric constant with increase in frequency. The Dielectric Constant values are observed to be decreasing with increasing frequency.

With PANI having two types of charged species i.e., one polaron/bipolaron and the others - bound charges (dipoles), a strong polarization arises in the system. This is assumed to happen because of the fact that the polaron/bipolaron is mobile and free to move along the chain and the dipoles have only restricted mobility giving rise to the space-charge polarization which explains that Dielectric Constant approaches saturation value at higher frequencies**.**

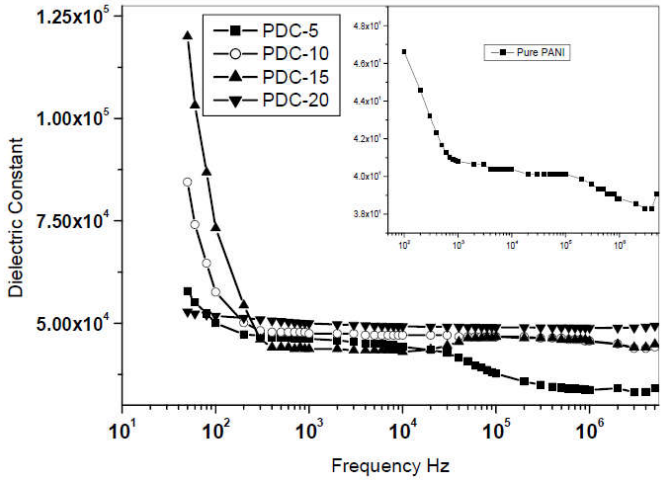

Figure 7 Frequency dependent dielectric constant of PANI(inset figure) and PANI composites a)PDC-5 b) PDC-10 c) PDC-15 d)PDC-20.

At saturated level, PDC-20 exhibits highest dielectric constant. Inset of the Fig.7 shows variation of dielectric constant with respect to frequency for Pure PANI. Composites show higher dielectric constant than pure PANI. Dielectric constant "ε" is given by the equation

$$\varepsilon\varepsilon = \frac{C_{gb}}{C_0} \qquad \text{---------- 2}$$

C_{gb} is the grain boundary capacitance and C_0 capacitance in vacuum.

The above equation shows that Dielectric constant is dependent on grain boundary capacitance [40]. As the concentration of CCN increases the amount of charge carriers decreases in the PANI/CCN composite, hence grain boundary capacitance decreases leading to the decrease in Dielectric constant value.

Dielectric Loss

Fig.8 shows Dielectric Loss property of the PDC composites. At lower frequency PDC-10 composites shows higher dielectric loss. As the frequency increases all the composites show saturated dielectric loss, at saturated level almost all samples show saturated dielectric loss. Inset of the Fig.8 shows dielectric loss for pure PANI.

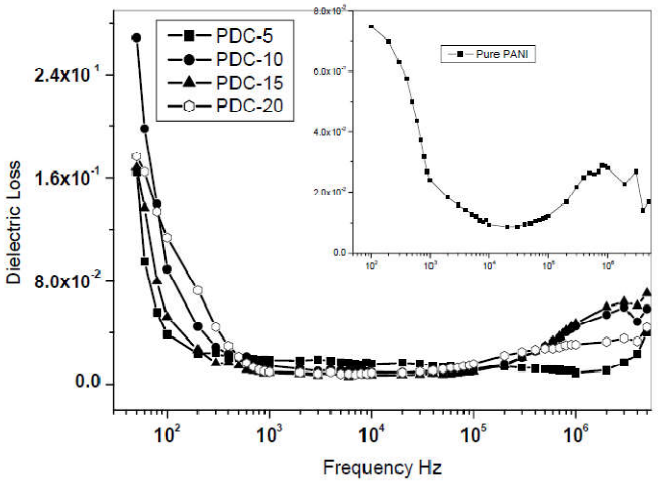

Figure 8 Frequency dependent dielectric loss of PANI(inset figure) and PANI composites a) PDC-5 b) PDC-10 c) PDC-15 d)PDC-20.

Composites show higher dielectric loss than pure PANI. Here same behavior is observed as in case of Dielectric constant of the nanocomposites.

Gas sensing studies

The measurement of gas sensing property of a sensor is done as explained elsewhere [41]. In a typical measurement, PANI/CCN composite is first calcined at 100 ^{0}C after which it is mixed with 2% PVA binder and then coated on to alumina tube substrate of length 15 mm and diameter 5 mm which is provided with a pair of Pt electrodes at two ends for electrical contact are shown in Fig 9. The sensor is sintered at low temperature for 2 hr to make it rigid for imparting ceramic properties**.** Decomposition of PVA takes place followed by strengthening of sensor element. This sensor element is fixed inside an aluminium specimen chamber with a nichrome heater and chromel-alumel thermocouple. Different test gases are introduced with the help of a syringe in this chamber. The input voltage of 10V is applied. The output is connected to Keithley automatic multimeter. The output voltage across the sensor with increasing temperature is measured and resistance of the element is calculated. The sensitivity 'S' of the sensor is defined as the ratio of change in the electrical resistance in air and the gas, $\Delta R=R_a-R_g$, to the electrical resistance in air R_a

i.e., $S= (R_a- R_g)/ R_a$ ----------3

This is also referred to as the fractional baseline manipulation response which is the most general method used to measure the sensor activity of conducting gas sensors [42].

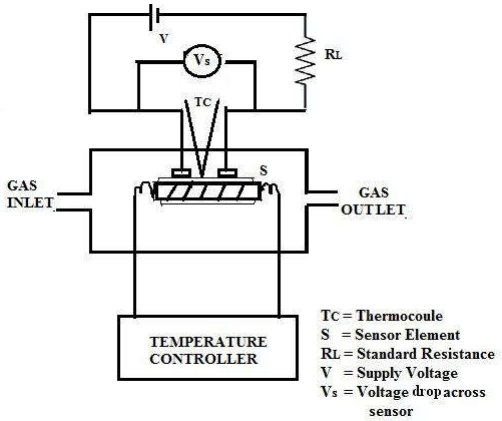

Figure 9 The experimental set up for the measurement of sensor activity.

Gas sensing property of PANI/CCN sensor for NH_3, CO_2 and CH_3OH gas is studied. The responses of composites PDC-5, PDC-10, PDC-15 and PDC-20 are recorded for all the gases shown in the Fig.10.

The response of PDC-15 is notable and the description is as follows. The variation in the response of the sensor element to these gases at 100 ppm concentration with temperature is shown in Fig.11. The resistance of the sensor is measured in air atmosphere before introducing any gas in the chamber R_a. Then a quantity of 2 mL, 3 mL, 5 mL and 7 ml of these gases is inserted in the chamber of 20 mL. The response is recorded and finally it is optimized for 5 mL at which response of the sensor is optimum. Highest sensitivity of 0.18 is recorded for methanol at 130^0C.

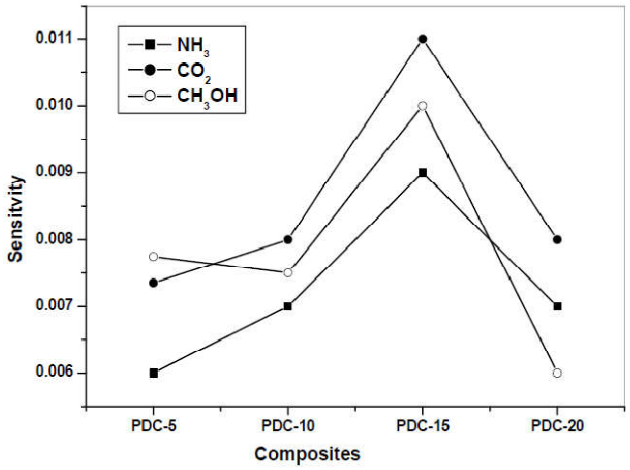

Figure 10 Sensitivity of PANI composites fordifferent gases at room temperature (30 ^{0}C).

The gases NH_3 and CO_2 recorded almost same value of sensitivity i.e., 0.14 at same temperature (130^0C) as that of CH_3OH. The above study of sensor characteristics shows that the sensitivity towards these three gases is nearly the same, though slightly greater response is noted for methane at the same operating temperatures. The gases showed a maximum response at around 130 ^{0}C.

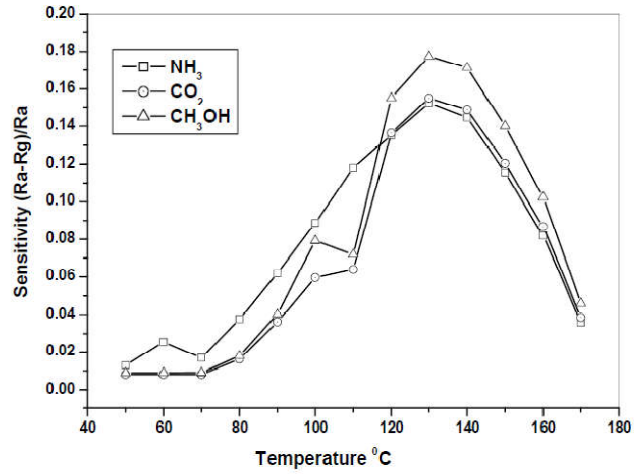

Figure 11 Sensitivity of different gases as a function of operating temperature for (a) NH_3 (b) CO_2 (c) CH_3OH.

B. Baruwati *et.al*. assumed that the gas sensor property of semiconductor is a surface controlled process[43]. She further stated that n-type semiconducting oxide in air (species like O^-, O^{-2}, O_2^-) creates localize mobile electrons, surface of the individual particles and inter-granular regions depletion layer is creating. The electron localization process is destroyed by the reaction of the test gas with the charged oxygen species which gives rise to the change in resistance[44]. Mei Chen *et.al*. concluded that the gas sensing properties of sensors depend upon crystal defect structure since the same determines the electronic properties of semiconductors[45].C V Gopal Reddy *et.al*., explained this phenomenon on the basis of Electron-hole pair mechanism in which holes are the majority carriers responsible for the conductivity. They also hinted that smaller crystallite size promotes the solid-gas interaction due to enhanced surface area of nano sized metal oxides[46].

In case of conducting polymer, the sensing mechanism takes place in a different manner wherein polarons obtained by doping and dedoping play the role of crystal defect structure. Among the three forms of PANI, emeraldine salt form is the conducting one. The sensor activity of polyaniline depends on the degree of protonic acid doping and the redox state of the polymer chain[47,48]. If a gas injected on PANI or composites, the reduction and oxidation state on the surface is altered which affects the conductivity and hence the sensitivity of PANI. Reduction or oxidation of the conducting polyaniline emeraldine salt change the number of electrons of polyaniline backbone converting the polymer to the insulating leucoemeraldine or pernigraniline states, respectively. Hence, redox active chemicals and gases will change the PANI conductivity by changing its inherent oxidation state. As we have confirmed from the PDC-15 structure and morphological properties are unique in comparison with the other samples. These morphological properties follows the same metal oxide and conducting polymer contribution for the high sensitivity.

When the metal oxides are introduced into the matrix of the CPs, there occurs unique phenomenon of gas sensing due to the combination of excellent properties of both metal oxides and CPs. And also it can be deduced from all these studies that the sensor response of PANI/CCN nanocomposite sensor is governed by the factors such as charged oxygen species, the rates of adsorption and desorption, the charge carrier concentration, degree of protonic acid doping and the redox state of the polymer. Future scope for the same materials are planed prepare thin films and tuning to sense the gas at lower or ambient temperature.

CONCLUSIONS

$CuCeO_2$ nanoparticles are synthesized by UGC method. The synthesized CCN are blended with PANI by in situ chemical oxidative polymerization method to get PDC composites. The resulting compositesare characterized. FTIR indicates weak interactive forces of attraction between CCN and the polymer. The particle size of the nanocomposites is computed from Scherer's equation using intense peaks from XRD. The average particles size ranges from 55.63 nm to 63.43 nm and confirms the presence of $CuCeO_2$and polyaniline and verified by WH method which supports the fact that strain is induced in composites during polymerization. SEM images reveal the encapsulation of the metal oxide by PANI and cluster formation. PDC-15 composite shows high conductivity and dielectric constant which may be due particle size. Dielectric behaviour of the nanocomposites wherein the Dielectric constant and Dielectric Loss decrease is due to the space-charge polarization and decrease in grain boundary capacitance. Gas Sensor activity of the above synthesized

composites are studied and results are analysed with the particle size, adsorption and desorption of the charge carrier concentration of the composites.

Acknowledgement

Authors are thankful to Department of chemistry SDM college of Engg. Dharwad and Acharya Institute of Technology Bangaluru For providing the facility.

References

1. K. Mallick, M. Witcomb, M. Scurrell, Fabrication of a nanostructured gold-polymer composite material, *Eur. Phys. J*. E 20 (2006) 347-353.
2. H. Kebichea, D. Debarnota, A. Merzoukib, A. Poncin-Epaillard, N. Haddaoui, Relationship between ammonia sensing properties of polyaniline nanostructures and their deposition and synthesis methods, *Analytica Chimica Acta* 737 (2012) 64-71.
3. P.C. Ramamurthy, A.M. Malshe, W.R. Harrell, R.V. Gregory, K. McGuire, A.M. Rao, Polyaniline/single-walled carbon nanotube composite electronic device, Solid-State Electron 48 (2004) 2019-2024.
4. S. Kuwabata, N. Takahashi, S. Hirao, H. Yoneyama, Light image formations on deprotonated polyaniline films containing titania particles, *Chem. Mater*. 5 (1993) 437-441.
5. M. Ilieva, S. Ivanov, V. Tsakova, Electrochemical synthesis and characterization of TiO_2-polyaniline composite layers, *J. Appl. Electrochem*. 38 (2008) 63-69.
6. S.W. Phang, M. Tadokoro, J. Watanabe, N. Kuramoto, Microwave absorption behaviors of polyaniline nanocomposites containing TiO_2 nanoparticles, *Curr.Appl.Phys.* 8(2008) 391-394.
7. M. Nagaraja, J. Pattar, N. Shashank, J. Manjanna, Y. Kamada, K. Rajanna, .H.M. Mahesh, Electrical structural and magnetic properties of polyaniline/pTSA-TiO_2 nanocomposites, *Synth. Met*. 159 (2009) 718-722.
8. C. Basavaraja, R. Pierson, T.K. Vishnuvardhan, D.S. Huh,Characterization and electrical behavior of polyaniline–poly-***N***-isopropylacrylamide-co-acrylic acid/alumina aqueous dispersions in presence of dodecyl benzenesulfonic acid, *Eur.Polym. J*.44(2008)1556-1566.
9. A. Katoch, M. Burkhart, T. Hwang, S.S. Kim, Synthesis of polyaniline/TiO2 hybrid nanoplates via a sol-gel chemical method, *Cheml. Eng. J*. 192 (2012) 262-298.
10. P. Paulraj, N. Janaki, S. Sandhya, K. Pandian, Single pot synthesis of polyaniline protected silver nanoparticles by interfacial polymerization and study its application on electrochemical oxidation of hydrazine, Colloids and Surfaces A:Physicochem. *Eng. Aspects* 377 (2011) 28-34.
11. Y.O. Kang, S.H. Choi, A. Gopalan, K.P. Lee, H.D. Kang, Y.S. Song, One-pot synthesis of a few nanocomposites with poly(*N*-vinylcarbazole) and CdS, Ag, Pd_{50}-Ag_{50}, and Pt_{50}-Ru_{50} nanoparticles with γ irradiation, *J. Appl. Polym. Sci*. 100 (2006) 1809-1815.
12. T.N. Ravishankar, T. Ramakrishnappa, G. Nagaraju, H. Rajanaika, Synthesis, characterization of CeO2 nanoparticles via solution combustion method for photocatalytic and antibacterial activity studies, *Chemistry Open* 4 (2015) 146.
13. J.P. Nair, E. Wachtel, I. Lubomirsky, J. Fleig, J. Maier, Anomalous Expansion of CeO_2 Nanocrystalline Membranes, *Adv. Mater*. 15 (2003) 2077-2081.
14. P. Bera, S.T. Aruna, K.C. Patil, M.S. Hegde,,Studies on Cu/CeO_2: A New NO Reduction Catalyst, *J. Catal*.186 (1999) 36-44.
15. R.K. Pati, I.C. Lee, S. Hou, O. Akhuemonkhan, K.J. Gaskell, Q. Wang, A.I. Frenkel, D. Chu, L.G. Salamanca-Riba, S.H. Ehrman, Flame synthesis of nanosized Cu-Ce-O, Ni-Ce-O and Fe-Ce-O catalysts for the Water-Gas shift (WGS) reaction, *Appl.Mater.Interfaces* 1 (2009) 2624-2635.
16. J. Kaspar, P. Fornasiero, M. Graziani,Use of CeO2-based oxides in the three-way catalysis, Catal. Today50 (1999) 285-298.
17. M. Nolan, V.S. Verdugo, H. Metiu, Vacancy formation and CO adsorption on gold-doped ceria surfaces, *Surf. Sci*., 602 (2008) 2734-2742.
18. S.T. Aruna, A.S. Mukasyan, Combustion synthesis and nanomaterials 2008, *Curr. Opin. Solid State and Mater. Sci.* 12 (2008) 44-50.
19. L. Szabova, M.F. Camellone, M. Huang, V. Matolin, S. Fabris, Thermodynamic, electronic and structural properties of Cu/CeO2 surfaces and interfaces from first-principles DFT+U calculations, *J. Chem.Phys*.133 (2010) (23):234705.
20. T. Masui, H. Hirai, N. Imanaka, G. Adachi, T. Sakata, H. Mori, Synthesis of cerium oxide nanoparticles by hydrothermal crystallization with citric acid, *J. Mater. Sci. Lett.* 21 (2002) 489-491.
21. W.K. Han, J.W. Choi, G.H. Hwang, S.J. Hong, J.S. Lee, Fabrication of Cu nano particles by direct electrochemical reduction from CuO nano particles, *Appl. Surface Sci*. 252 (2006) 2832-2838.
22. M.S. Usman, Z.K. Shameli, N.Z. Salama, N.A. Ibrahim, Synthesis, characterization, and antimicrobial properties of copper nanoparticles, I *J. Nanomed*. 17 (2013) 4467-4479.
23. L. Kundakovic, M. Flytzani-Stephanopoulos, Cu- and Ag-modified cerium oxide catalysts for methane oxidation, *J. Catal*., 179 (1998) 203-221.
24. J. Lee, E. Kim, Effect of Structural and Morphological Changes on the Conductivity of Stretched PANI-DBSA/HIPS Film, *Bull. Korean Chem. Soc*. 32 (2011) 2661-2665.
25. S.D. Nagesa, M. Revanaiddappa, C. Basavaraja, T. Suresh, S.C.Raghavendra, DC conductivity studies of doped PANI-WO_3 nanocomposites, *Indian J. Eng. Mater. Sci.* 20 (2013) 435-442.
26. S. Parveen, C. Veena, Structural, spectral and thermal properties of bulky organic sulfonic acids doped polyanilines and antistatic performance of its melt blend, *Indian J. Pure Appl. Phy*. 53 (2015) 320.
27. C. Mousty, Sensors and biosensors based on clay-modified electrodes-new trends, *Appl. Clay Sci*. 27 (2004) 159-177.
28. F. Leroux, C. Taviot-Gueho, Fine tuning between organic and inorganic host structure: new trends in

layered double hydroxide hybrid assemblies*, J. Mater. Chem.* 15(2005) 3628-3642.
29. S. Wang, Y. Kang, L. Wang, H, Zhang, Y. Wang, Y. Wang, Organic/inorganic hybrid sensors: A review, Sens. Actuators: B 182 (2013) 467- 481.
30. E. Smela, Microfabrication of PPy microactuators and other conjugated polymer devices, *J. Micromech. Microengg*. 9 (1999) 1-18.
31. Y.S. Negi, P.V. Adhyapak, Development in polyaniline conducting polymers, *J. of Macromol. Sci. Polym. R*ev. 42 (2002) 35-53.
32. S. Brady, K.T. Lau, W. Megill, G.G. Wallace, D. Diamond, The development and characterisation of conducting polymeric-based sensing devices, *Synth.Met.* 154 (2005) 25-28.
33. G.G. Wallace, G.M. Spinks, A.P. Kane-Maguire, P.R. Tesdale, Conductive Electroactive Polymers: Intelligent Materials Systems, Third Ed. CRC Press, London, 2008.
34. S.S. Joshi, T.P. Gujar, V.R. Shinde, C.D. Lokhande, Fabrication of n-CdTe/ppolyaniline heterojunction-based room temperature LPG sensor, Sens. Actuators:B 132 (2008) 349-355.
35. M.K. Ram, O. Yavuz, M. Aldissi, NO_2 gas sensing based on ordered ultrathin films of conducting polymer and its nanocomposites, *Synth. Met*. 151 (2005) 77-84.
36. Y. Wu, S.X. Xing, J.C. Fu, Examining the use of TiO_2 to enhance the NH_3 sensitivity of polypyrrole films*, J. Appl. Polym. Sci.* 118 (2010) 3351-3356.
37. B.H. Shambharkar, S.S. Umare, Synthesis and characterization of polyaniline/NiO nanocomposite, *J. Appl. Polym. Sc*i. 122 (2011) 1905-1912.
38. A.K. Zak, A.W.H. Majid, M.E. Abrishami, R. Yousefi, X-ray analysis of ZnO nanoparticles by Williamson-Hall and size-strain plot Methods, *Solid-State Sc*i. 13 (2011) 251-256.
39. K. Pandey, M.M. Dwivedi, M. Singh, S.L. Agrawal, Studies of dielectric relaxation and a.c. conductivity in $[(100-x)PEO + xNH_4SCN]$: Al-Zn ferrite nano composite polymer electrolyte, *J. Polym. Res*.17 (2010) 127.
40. T.K. Vishnuvardhan, V.R. Kulkarni, C. Basavaraja, S. C. Raghavendra, Synthesis, characterization and a.c. conductivity of polypyrrole/Y_2O_3 composites, *Bull. Mater. Sci.* 29 (2006) 77-83.
41. L. Satyanarayana, C.V. Gopal Reddy, S.V. Manorama, V.J. Rao, Liquid-petroleum-gas sensor based on a spinel semiconductor, $ZnGa_2O_4$, Sensors and Actuators B: Chem. (1999) 1-7.
42. T.C. Pearce, S.S. Schiffman, H.T. Nagle, J.W. Gardner, Handbook of Machine Olfaction, Wiley-VCH, Weinheim, 2003.
43. B. Baruwati, D. Kishore Kumar, S.V. Manorama, Hydrothermal synthesis of highly crystalline ZnO nanoparticles: A competitive sensor for LPG and EtOH, Sensors and Actuators B 119 (2006) 676-682.
44. J. Jose, A. Khadar, Impedance spectroscopic analysis of AC response of nanophase ZnO and ZnO-Al_2O_3 nanocomposites, *Nanostruct. Mater*. 11 (1999) 1091-1099.
45. M. Chen, Z. Wang, D. Han, F. Gu, G. Guo, Porous ZnO Polygonal Nanoflakes: Synthesis, Use in High-Sensitivity NO_2 Gas Sensor, and Proposed Mechanism of Gas Sensing*, J. Phys. Chem*. C 115 (2011) 12763-12773.
46. C.V. Gopal Reddy, S.V. Manorama, V.J. Rao, Semiconducting gas sensor for chlorine based on inverse spinel nickel ferrite, Sensors and Actuators B:chem. 55 (1999) 90-95.
47. A.Z. Md Sadek, Investigation of Nanostructured Semiconducting Metal Oxide and Conducting Polymer Thin Films for Gas Sensing Applications, Thesis submitted to RMIT University, School of Electrical and Computer Engineering, RMIT University, Melbourne, Australia, April, 2008.
48. J.C. Chiang, A.G. MacDiarmid, Polyaniline: Protonic acid doping of the emeraldine form to the metallic regime, *Synth. Met*. 13 (1986) 193-205.

How to cite this article:

Rajashekhar Badiger *et al* (2017) 'Morphology and Sensor Property of Olyaniline/Cuceo2 nanocomposites', *International Journal of Current Advanced Research,* 06(12), pp. 8249-8256. DOI: http://dx.doi.org/10.24327/ijcar.2017.8256.1320

****